Editors' Suggestion

Precision Measurement of Neutrino Oscillation Parameters with 10 Years of Data from the NOvA Experiment

S. Abubakar,[12] M. A. Acero,[2] B. Acharya,[32] P. Adamson,[13] N. Anfimov,[27] A. Antoshkin,[27] E. Arrieta-Diaz,[28] L. Asquith,[41] A. Aurisano,[7] D. Azevedo,[15] A. Back,[21,25] N. Balashov,[27] P. Baldi,[26] B. A. Bambah,[18] E. F. Bannister,[41] A. Barros,[2] A. Bat,[3,12] R. Bernstein,[13] T. J. C. Bezerra,[41] V. Bhatnagar,[35] B. Bhuyan,[16] J. Bian,[26,31] A. C. Booth,[37,41] R. Bowles,[21] B. Brahma,[19] C. Bromberg,[29] N. Buchanan,[9] A. Butkevich,[23] S. Calvez,[9] T. J. Carroll,[43,49] E. Catano-Mur,[48] J. P. Cesar,[43] S. Chaudhary,[16] R. Chirco,[20] S. Choate,[50] B. C. Choudhary,[11] O. T. K. Chow,[37] A. Christensen,[9] M. F. Cicala,[45] T. E. Coan,[40] T. Contreras,[13] A. Cooleybeck,[49] D. Coveyou,[46] L. Cremonesi,[37] G. S. Davies,[32] P. F. Derwent,[13] P. Ding,[13] Z. Djurcic,[1] K. Dobbs,[17] M. Dolce,[47] D. Dueñas Tonguino,[7] E. C. Dukes,[46] A. Dye,[32] R. Ehrlich,[46] E. Ewart,[21] G. J. Feldman,[51] P. Filip,[24] M. J. Frank,[38] H. R. Gallagher,[44] F. Gao,[36] A. Giri,[19] R. A. Gomes,[15] M. C. Goodman,[1] R. Group,[46] A. Habig,[30] F. Hakl,[22] J. Hartnell,[41] R. Hatcher,[13] J. M. Hays,[37] M. He,[17] K. Heller,[31] V. Hewes,[7] A. Himmel,[13] T. Horoho,[46] X. Huang,[32] A. Ivanova,[27] B. Jargowsky,[26] I. Kakorin,[27] A. Kalitkina,[27] D. M. Kaplan,[20] A. Khanam,[42] B. Kirezli,[12] J. Kleykamp,[32] O. Klimov,[27] L. W. Koerner,[17] L. Kolupaeva,[27] R. Kralik,[41] A. Kumar,[35] C. D. Kuruppu,[39] V. Kus,[10] T. Lackey,[13,21] K. Lang,[43] J. Lesmeister,[17] A. Lister,[49] J. Liu,[26] J. A. Lock,[41] M. MacMahon,[45] S. Magill,[1] W. A. Mann,[44] M. T. Manoharan,[8] M. Manrique Plata,[21] M. L. Marshak,[31] M. Martinez-Casales,[13,25] V. Matveev,[23] A. Medhi,[16] B. Mehta,[35] M. D. Messier,[21] H. Meyer,[47] T. Miao,[13] V. Mikola,[45] W. H. Miller,[31] S. R. Mishra,[39] A. Mislivec,[31] R. Mohanta,[18] A. Moren,[30] A. Morozova,[27] W. Mu,[13] L. Mualem,[5] M. Muether,[47] K. Mulder,[45] C. Murthy,[43] D. Myers,[43] J. Nachtman,[50] D. Naples,[36] S. Nelleri,[8] J. K. Nelson,[48] O. Neogi,[50] R. Nichol,[45] E. Niner,[13] A. Norman,[13] A. Norrick,[13] H. Oh,[7] A. Olshevskiy,[27] T. Olson,[17] M. Ozkaynak,[45] A. Pal,[34] J. Paley,[13] L. Panda,[34] R. B. Patterson,[5] G. Pawloski,[31] R. Petti,[39] R. K. Plunkett,[13] L. R. Prais,[32,7] A. Rafique,[1] V. Raj,[5] M. Rajaoalisoa,[7] B. Ramson,[13] B. Rebel,[49] C. Reynolds,[37] E. Robles,[26] P. Roy,[47] O. Samoylov,[27] M. C. Sanchez,[14,25] S. Sánchez Falero,[25] P. Shanahan,[13] P. Sharma,[35] A. Sheshukov,[27] A. Shmakov,[26] W. Shorrock,[41] S. Shukla,[4] I. Singh,[11] P. Singh,[37,11] V. Singh,[4] S. Singh Chhibra,[37] D. K. Singha,[18] E. Smith,[21] J. Smolik,[10] P. Snopok,[20] N. Solomey,[47] A. Sousa,[7] K. Soustruznik,[6] M. Strait,[13,31] C. Sullivan,[44] L. Suter,[13] A. Sutton,[14,25] K. Sutton,[5] S. K. Swain,[34] A. Sztuc,[45] N. Talukdar,[39] P. Tas,[6] T. Thakore,[7] J. Thomas,[45] E. Tiras,[12,25] M. Titus,[8] Y. Torun,[20] D. Tran,[17] J. Trokan-Tenorio,[48] J. Urheim,[21] B. Utt,[31] P. Vahle,[48] Z. Vallari,[33] K. J. Vockerodt,[37] A. V. Waldron,[37] M. Wallbank,[7,13] T. K. Warburton,[25] C. Weber,[31] M. Wetstein,[25] D. Whittington,[42] D. A. Wickremasinghe,[13] J. Wolcott,[44] S. Wu,[31] W. Wu,[26] W. Wu,[36] Y. Xiao,[26] B. Yaeggy,[7] A. Yahaya,[47] A. Yankelevich,[26] K. Yonehara,[13] S. Zadorozhnyy,[23] J. Zalesak,[24] and R. Zwaska[13]

(The NOvA Collaboration)

[1]*Argonne National Laboratory, Argonne, Illinois 60439, USA*
[2]*Universidad del Atlantico, Carrera 30 No. 8-49, Puerto Colombia, Atlantico, Colombia*
[3]*Bandirma Onyedi Eylül University, Faculty of Engineering and Natural Sciences, Engineering Sciences Department, 10200, Bandirma, Balıkesir, Turkey*
[4]*Department of Physics, Institute of Science, Banaras Hindu University, Varanasi 221 005, India*
[5]*California Institute of Technology, Pasadena, California 91125, USA*
[6]*Charles University, Faculty of Mathematics and Physics, Institute of Particle and Nuclear Physics, Prague, Czech Republic*
[7]*Department of Physics, University of Cincinnati, Cincinnati, Ohio 45221, USA*
[8]*Department of Physics, Cochin University of Science and Technology, Kochi 682 022, India*
[9]*Department of Physics, Colorado State University, Fort Collins, Colorado 80523-1875, USA*
[10]*Czech Technical University in Prague, Brehova 7, 115 19 Prague 1, Czech Republic*
[11]*Department of Physics and Astrophysics, University of Delhi, Delhi 110007, India*
[12]*Department of Physics, Erciyes University, Kayseri 38030, Turkey*
[13]*Fermi National Accelerator Laboratory, Batavia, Illinois 60510, USA*
[14]*Florida State University, Tallahassee, Florida 32306, USA*
[15]*Instituto de Física, Universidade Federal de Goiás, Goiânia, Goiás 74690-900, Brazil*
[16]*Department of Physics, IIT Guwahati, Guwahati 781 039, India*
[17]*Department of Physics, University of Houston, Houston, Texas 77204, USA*
[18]*School of Physics, University of Hyderabad, Hyderabad 500 046, India*
[19]*Department of Physics, IIT Hyderabad, Hyderabad 502 205, India*
[20]*Illinois Institute of Technology, Chicago, Illinois 60616, USA*

[21]Indiana University, Bloomington, Indiana 47405, USA
[22]Institute of Computer Science, The Czech Academy of Sciences, 182 07 Prague, Czech Republic
[23]Institute for Nuclear Research of Russia, Academy of Sciences 7a, 60th October Anniversary prospect, Moscow 117312, Russia
[24]Institute of Physics, The Czech Academy of Sciences, 182 21 Prague, Czech Republic
[25]Department of Physics and Astronomy, Iowa State University, Ames, Iowa 50011, USA
[26]Department of Physics and Astronomy, University of California at Irvine, Irvine, California 92697, USA
[27]Joint Institute for Nuclear Research, Dubna, Moscow region 141980, Russia
[28]Universidad del Magdalena, Carrera 32 No 22-08, Santa Marta, Colombia
[29]Department of Physics and Astronomy, Michigan State University, East Lansing, Michigan 48824, USA
[30]Department of Physics and Astronomy, University of Minnesota Duluth, Duluth, Minnesota 55812, USA
[31]School of Physics and Astronomy, University of Minnesota Twin Cities, Minneapolis, Minnesota 55455, USA
[32]University of Mississippi, University, Mississippi 38677, USA
[33]Department of Physics, Ohio State University, Columbus, Ohio 43210, USA
[34]National Institute of Science Education and Research, An OCC of Homi Bhabha National Institute, Bhubaneswar, Odisha, India
[35]Department of Physics, Panjab University, Chandigarh 160 014, India
[36]Department of Physics, University of Pittsburgh, Pittsburgh, Pennsylvania 15260, USA
[37]Particle Physics Research Centre, Department of Physics and Astronomy, Queen Mary University of London, London E1 4NS, United Kingdom
[38]Department of Physics, University of South Alabama, Mobile, Alabama 36688, USA
[39]Department of Physics and Astronomy, University of South Carolina, Columbia, South Carolina 29208, USA
[40]Department of Physics, Southern Methodist University, Dallas, Texas 75275, USA
[41]Department of Physics and Astronomy, University of Sussex, Falmer, Brighton BN1 9QH, United Kingdom
[42]Department of Physics, Syracuse University, Syracuse, New York 13210, USA
[43]Department of Physics, University of Texas at Austin, Austin, Texas 78712, USA
[44]Department of Physics and Astronomy, Tufts University, Medford, Massachusetts 02155, USA
[45]Physics and Astronomy Department, University College London, Gower Street, London WC1E 6BT, United Kingdom
[46]Department of Physics, University of Virginia, Charlottesville, Virginia 22904, USA
[47]Department of Mathematics, Statistics, and Physics, Wichita State University, Wichita, Kansas 67260, USA
[48]Department of Physics, William & Mary, Williamsburg, Virginia 23187, USA
[49]Department of Physics, University of Wisconsin-Madison, Madison, Wisconsin 53706, USA
[50]Department of Physics and Astronomy, University of Iowa, Iowa City, Iowa 52242, USA
[51]Department of Physics, Harvard University, Cambridge, Massachusetts 02138, USA

(Received 9 September 2025; accepted 26 November 2025; published 8 January 2026)

This Letter reports measurements of muon-neutrino disappearance and electron-neutrino appearance and the corresponding antineutrino processes between the two NOvA detectors in the NuMI neutrino beam. These measurements use a dataset with double the neutrino mode beam exposure that was previously analyzed, along with improved simulation and analysis techniques. A joint fit to these samples in the three-flavor paradigm results in the most precise single-experiment constraint on the atmospheric neutrino mass splitting, $\Delta m^2_{32} = 2.431^{+0.036}_{-0.034}(-2.479^{+0.036}_{-0.036}) \times 10^{-3}$ eV^2 if the mass ordering is normal (inverted). In both orderings, a region close to maximal mixing with $\sin^2\theta_{23} = 0.55^{+0.02}_{-0.06}$ is preferred. The NOvA data show a mild preference for the normal mass ordering with a Bayes factor of 2.4 (corresponding to 70% of the posterior probability), indicating that the normal ordering is 2.4 times more probable than the inverted ordering. When incorporating a 2D $\Delta m^2_{32} - \sin^2 2\theta_{13}$ constraint based on Daya Bay data, this preference strengthens to a Bayes factor of 6.6 (87%).

DOI: 10.1103/x53y-2b86

Neutrino oscillations [1,2] describe the phenomenon by which a neutrino produced in a particular flavor at one point in spacetime can subsequently be detected as a different flavor. This flavor transformation occurs due to mixing [3] between the flavor eigenstates (ν_e, ν_μ, ν_τ) and the mass eigenstates (ν_1, ν_2, ν_3). For a unitary mixing matrix, neutrino oscillation probabilities can be characterized by three mixing angles (θ_{12}, θ_{13}, θ_{23}), the charge-parity (CP) violation phase (δ_{CP}), and two nonzero mass splittings (Δm^2_{21} and Δm^2_{32}, where $\Delta m^2_{ij} \equiv m^2_i - m^2_j$). Although intensively studied for over 25 years [4–14], key aspects

Published by the American Physical Society under the terms of the Creative Commons Attribution 4.0 International license. Further distribution of this work must maintain attribution to the author(s) and the published article's title, journal citation, and DOI. Funded by SCOAP^3.

of neutrino oscillations remain poorly constrained or entirely unknown. These include the determination of the neutrino mass ordering (whether Δm^2_{32} is positive or negative), the octant of θ_{23} (whether θ_{23} is less than or greater than $\pi/4$), and the existence of CP violation in the neutrino sector (quantified by δ_{CP}).

Resolving these open questions and achieving precise measurements of the mixing parameters have broad implications for fundamental particle physics. The neutrino mass ordering (MO), i.e., whether the third mass eigenstate is heavier (normal MO) or lighter (inverted MO) than the others, is crucial for neutrino mass generation models, understanding supernova neutrino fluxes, and the search for neutrinoless double beta decay (see Refs. [15–17] and references therein). The mixing angle θ_{23} governs the potential symmetry between the ν_μ and ν_τ components of ν_3. The value of δ_{CP} is relevant to theories explaining the matter-antimatter asymmetry of the Universe via leptogenesis [18,19].

The NuMI Off-axis ν_e Appearance (NOvA) experiment [20] is designed to study neutrino oscillations using Fermilab's NuMI beam [21] and two functionally identical detectors separated by a long baseline. NOvA measures $P(\nu_\mu \to \nu_\mu)$ and $P(\nu_\mu \to \nu_e)$, along with their antineutrino counterparts, by comparing unoscillated neutrino interactions observed at the Near Detector (ND) with oscillated interactions at the Far Detector (FD). The ND and FD are located 1 km and 810 km, respectively, from the neutrino beam target, with both detectors positioned 14.6 mrad off axis, resulting in a narrow energy band peaked at 1.8 GeV.

The Fermilab Main Injector accelerator delivers 120 GeV protons that strike a 1.2 m graphite target, producing a secondary hadron beam. The hadrons are focused by magnetic horns and directed into a decay pipe, where they decay into neutrinos. Integrated over the 1–5 GeV energy range, the unoscillated beam is 94% pure ν_μ in neutrino mode and 93% pure $\bar{\nu}_\mu$ in antineutrino mode. The wrong-sign (WS) component, i.e., antineutrinos in neutrino mode and neutrinos in antineutrino mode, is 5% (6%) contamination in the neutrino (antineutrino) mode. The remaining flux is less than 1% intrinsic ν_e and $\bar{\nu}_e$ for both modes.

Both detectors are low-Z tracking calorimeters composed of PVC cells with a cross-sectional area of 6.6×3.9 cm^2, corresponding to a depth of 0.18 radiation lengths and, in the transverse direction, 0.4 Molière radii [22] with lengths of 15.5 m (3.9 m) in the FD (ND). These cells are assembled into planes alternating between vertical and horizontal orientations, enabling 3D event reconstruction. Cells are filled with an organic scintillator (62% of total detector mass) based on mineral oil with 5% admixture of pseudocumene [23]. Scintillation light, along with a smaller amount of Cherenkov light, is collected by wavelength-shifting fibers looping through each cell with both fiber ends connected to a single pixel on an avalanche photodiode. The ND, located 100 m underground, consists of 192 planes and features an additional downstream muon catcher composed of alternating steel and scintillator layers for a total active mass of 193 t. The 14 kt FD consists of 896 planes. Located on the surface with an overburden of 3.6 m water equivalent, the FD experiences a cosmic-ray flux of 130 kHz which constitutes the primary background. Data are recorded in a window centered around the 10 μs NuMI beam spill [24]. In addition, cosmic-ray data are recorded for use in calibration and background estimation.

The results presented in this Letter use data collected from February 6, 2014, to March 13, 2024, corresponding to a total FD neutrino (antineutrino) beam exposure of 26.61×10^{20} (12.50×10^{20}) protons on target (POT) over 885.53 s (322.59 s) of beam-on time. This is equivalent to a 96% increase in the neutrino-mode beam exposure relative to previous NOvA results [25,26], while the antineutrino-mode exposure remains unchanged.

This analysis builds on previous NOvA work [25], incorporating updated simulation, improved systematic uncertainty treatments, and reoptimized energy reconstruction and event selection.

The neutrino flux is predicted at the ND and FD using GEANT4 (v4.10) [27,28], which simulates particle production and transport through the NuMI beamline components, and reweighted using the Package to Predict the FluX (PPFX) [29] to incorporate external constraints from hadron production measurements [30–48]. Neutrino interactions are simulated using a custom model configuration of GENIE 3.0.6 [49,50] tuned to NOvA ND as well as external data. This tuning creates a NOvA-specific version of the València MEC model [51,52], which describes charged-current (CC) neutrino scattering from correlated nucleon pairs via meson exchange. The tune also uses pion-nucleus scattering data [53–59] to improve the simulation of final-state interactions modeled with the GENIE hN intranuclear cascade model [50]. Outgoing final-state particles from neutrino interactions are then propagated through the detectors using GEANT4 and a custom readout simulation [60].

Energy distributions of neutrino candidates are built from reconstructed interactions in both detectors, and for both beam modes, in data and simulation. Detector cells with energy deposits above threshold are grouped into events and subsequently classified as ν_e CC, ν_μ CC, neutral-current (NC), or cosmic candidates. This identification combines classical algorithms and deep-learning techniques such as a convolutional neural network, following the procedure established in the previous analysis [25]. The ν_e and ν_μ candidate samples include both beam-intrinsic and oscillated neutrinos in the FD, as well as WS neutrinos in each beam mode. They also contain misidentified events, primarily from NC interactions, cosmic rays, and other reconstruction failures. For brevity, $\nu_\mu(\bar{\nu}_\mu)$ is used to indicate the dominant component in the

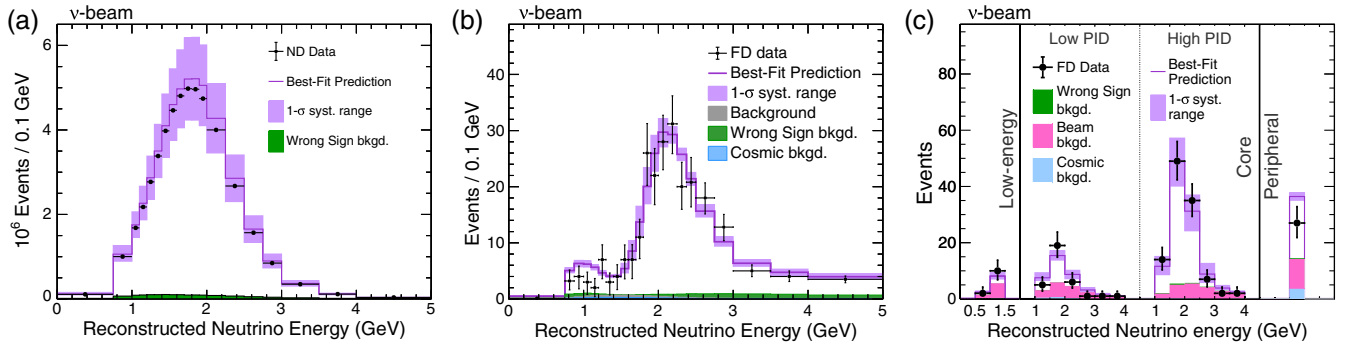


FIG. 1. Observed and predicted energy spectra, for ν_μ CC selected events in the ND (a) and FD (b), and for ν_e CC selected events in the FD (c). In the ν_μ spectra all subsamples have been combined, while in the ν_e spectra the four selections (low-energy, low PID, high PID, and peripheral) are shown separated. The best-fit prediction is extracted from the frequentist fit to the data with the Daya Bay 1D constraint on $\sin^2 2\theta_{13}$ [61]. The predicted FD spectra have smaller systematic errors than the ND spectrum as a result of the extrapolation procedure. The corresponding antineutrino spectra and quartile-separated samples are shown in the Supplemental Material [62].

neutrino (antineutrino) beam mode, although both modes contain a mix of ν_μ and $\bar{\nu}_\mu$.

The FD $\nu_\mu(\bar{\nu}_\mu)$ samples primarily probe the atmospheric oscillation parameters θ_{23} and $|\Delta m^2_{32}|$. The sensitivity from these samples depends on resolving the position and depth of the oscillation minimum (the "dip") in the reconstructed muon-neutrino energy spectrum, driven by $\overset{(-)}{\nu}_\mu \to \overset{(-)}{\nu}_\tau$ oscillations. Accurate estimation of the neutrino energy and careful choice of binning are critical to this measurement. This structure is visible in Fig. 1(b), which shows the energy distribution for neutrino beam mode. The neutrino energy is estimated as the sum of the muon energy, determined from track length, and hadronic energy, estimated from calorimetry. The mean energy resolution is 6%–13% for muon neutrinos and 5%–11% for muon antineutrinos, where the variation depends on the relative contribution of the hadronic energy component. To improve sensitivity to the dip structure, control systematic uncertainties, and account for acceptance differences between detectors, we use finer energy bins near the dip and divide the samples into bins of hadronic energy fraction and muon transverse momentum (p_T) [25].

The FD $\nu_e(\bar{\nu}_e)$ samples primarily probe the MO, δ_{CP} value, and θ_{23} octant. Electron-neutrino energy is estimated using a quadratic function of the hadronic and electromagnetic shower calorimetric energies. The overall energy resolution is approximately 11% for electron neutrinos and 9% for electron antineutrinos. The ν_e appearance measurement is sensitive to separating signal from background due to a higher relative background contribution than in the ν_μ samples. As a result, in addition to binning in reconstructed energy, two sub-samples of differing purities are constructed by grouping candidates into higher confidence (high PID) and lower confidence (low PID) bins, where PID denotes the particle identification score. These core bins are dominated by ν_e CC events, arising either from beam-intrinsic ν_e or from oscillated ν_μ.

The core bins are supplemented by the peripheral and, in neutrino beam mode, low-energy samples. As in the previous analysis [25], the peripheral selection adds high-confidence ν_e events with vertices outside the fiducial volume that may not deposit all their energy in the detector. This sample is treated as a single bin per beam mode rather than an energy distribution. Including these events increases the overall selection efficiency, which in turn provides a small improvement in sensitivity for certain combinations of δ_{CP} and mass ordering, despite the higher cosmic background expected from their positions in the detector. The low-energy sample, introduced in this analysis, covers the 0.5 to 1.5 GeV energy range, a previously underexplored region with significant sensitivity to the MO, now accessible due to the cumulative increase in neutrino beam exposure. Although statistics in this region remain limited, they are sufficient to improve the oscillation constraints. The sample is expected to suffer from high backgrounds, primarily because low-energy ν_e events are difficult to distinguish from NC interactions. To recover these events, candidates that fail the core selection are passed through a boosted decision tree optimized to identify events with low-energy electromagnetic showers from primary electrons. Current statistics in antineutrino mode are insufficient to define a similar selection.

Similar reconstruction and selection techniques are applied at the ND to construct candidate samples. In the neutrino beam mode, the ν_μ ND candidate distributions are used to constrain both the surviving ν_μ and appearing ν_e FD signal events while the ν_e ND candidates are used to constrain the various FD beam backgrounds in the ν_e sample. An analogous process is used for antineutrino beam samples. This data-driven method for building FD predictions prior to fitting the FD data to infer oscillation parameters is referred to as extrapolation and remains unchanged from the previous analysis [25]. This procedure is essential for mitigating the impact of systematic

uncertainties at the FD through the use of high-statistics ND data.

Systematic uncertainties are evaluated by varying model parameters in the simulation. The resulting shifted samples are processed through the same reconstruction, selection, and extrapolation procedures to assess their impact on the analysis. In this Letter, systematic uncertainties are grouped into categories including: neutrino flux, neutrino interaction cross sections, detector simulation, calibrations, lepton reconstruction, uncorrelated effects between the ND and FD, and neutron propagation in the detector. Most uncertainty estimates are unchanged from the previous analysis [25], although several new sources are now included.

In the cross-section category, new uncertainties are introduced to address potential mismodeling of pion production in the transition region between resonant (RES) and deep inelastic scattering (DIS), which is particularly challenging to model accurately [71]. GENIE's implementation assumes, as an ansatz, a fixed relationship between charged and neutral final states in this region. It also does not include uncertainties on the relative production rates of Δ and higher resonances. Therefore, additional uncertainties are included to account for possible variations in these quantities consistent with the current data [72,73]. For the detector model, the GEANT4Reweight package [74] is used to address uncertainties in the inelastic scattering of protons and pions produced during both primary neutrino interactions and subsequent secondary interactions [75]; these uncertainties are incorporated using principal component analysis [76]. In the neutron model category, a supplementary model, MENATE [77,78], is introduced to evaluate neutron detection uncertainties based on its differences with the default GEANT4 model [79]. MENATE provides improved modeling of neutron interactions in the 20–200 MeV range, where GEANT4 tends to underestimate energy deposition in scintillator detectors. Finally, following the update to NOvA's custom light model, two sets of systematic uncertainties are applied: a $\pm 5\%$ variation in the overall light yield and a $\pm 6.2\%$ scaling of the Cherenkov light-collection efficiency.

The extrapolation method reduces the impact of systematic uncertainties that are correlated between the detectors, particularly those related to flux and cross section. To provide a scale of this improvement, systematic uncertainties on the predicted total FD event rates drop from 12%–18% to 3%–6.5%, depending on the sample. Among the systematic uncertainties, those related to detector calibration contribute most to the uncertainties in Δm^2_{32} and $\sin^2\theta_{23}$, while cross-section systematics, especially those associated with the uncertainty in ν_e/ν_μ and $\bar{\nu}_e/\bar{\nu}_\mu$ cross section, primarily affect the δ_{CP} measurement. Table I summarizes the statistical and systematic contributions to the oscillation parameter uncertainties, showing that statistical errors are the dominant source of uncertainty for all measured parameters.

Oscillation parameters are inferred using a Poisson likelihood with a log-likelihood difference test statistic to compare the data and the corrected simulated FD spectra across various oscillation and systematic hypotheses. The analysis constrains $\sin^2\theta_{23}$, $\sin^2 2\theta_{13}$, Δm^2_{32}, and δ_{CP}, with both hypotheses of neutrino MO tested against the data. Because the sensitivity to θ_{13} is limited when fitting multiple oscillation parameters simultaneously, external input from the Daya Bay experiment [61] is incorporated to improve precision. Three treatments of θ_{13} are considered: no constraint (using only NOvA data), the Daya Bay $\sin^2 2\theta_{13}$ constraint (1D Daya Bay), and the two-dimensional Daya Bay constraint on $\sin^2 2\theta_{13}$ and Δm^2_{32} (2D Daya Bay). All other oscillation parameters are fixed to their values from PDG 2023 [80].

In this Letter, results are extracted using two complementary analyses—a Bayesian Markov Chain Monte Carlo (MCMC) method to compute posterior probability density distributions, and a frequentist analysis that yields

TABLE I. Systematic and statistical uncertainties on the oscillation parameters Δm^2_{32}, $\sin^2\theta_{23}$, and δ_{CP} are evaluated at the best-fit point extracted from a frequentist fit with the Daya Bay 1D constraint on $\sin^2 2\theta_{13}$ [61]. These predicted $\pm 1\sigma$ ranges are given as absolute error on the best-fit values. Asymmetric errors on δ_{CP} and $\sin^2\theta_{23}$ arise from limited sensitivity and degeneracy in parameters, leading to several highly probable regions that vary with the best-fit values.

Source	$\lvert\Delta m^2_{32}\rvert$ ($\times 10^{-5}$ eV^2)	$\sin^2\theta_{23}$ ($\times 10^{-3}$)	δ_{CP} ($\times 10^{-2}\pi$)
Beam flux	$+0.06/-0.12$	$+0.40/-0.75$	$+0.16/-1.00$
Calibration	$+1.40/-1.80$	$+3.20/-16.0$	$+1.70/-17.0$
Detector model	$+0.17/-0.27$	$+0.36/-3.90$	$+0.37/-3.30$
Lepton Reco.	$+0.90/-1.40$	$+2.70/-4.50$	$+0.61/-2.90$
ND—FD Uncor.	$+0.25/-0.34$	$+2.40/-2.50$	$+0.79/-4.00$
Cross sections	$+0.65/-1.10$	$+3.10/-5.10$	$+2.00/-9.70$
Neutron model	$+0.25/-0.39$	$+2.70/-0.49$	$+0.43/-1.30$
Systematic Unc.	$+1.70/-2.30$	$+6.60/-18.0$	$+2.90/-21.0$
Statistical Unc.	$+3.20/-4.40$	$+22.0/-85.0$	$+6.60/-74.0$

TABLE II. Observed and predicted numbers of ν_μ, ν_e and low-energy ν_e events in the neutrino beam, and $\bar{\nu}_\mu$ and $\bar{\nu}_e$ events in the antineutrino beam. The low PID, high PID, and peripheral samples have been combined in the $\nu_e(\bar{\nu}_e)$ columns, while the low-energy sample is shown separately due to its novel status in this analysis. WS is considered signal in the ν_μ and $\bar{\nu}_\mu$ samples, but background in the ν_e and $\bar{\nu}_e$ samples. We denote as others the sum of all remaining oscillation channels that are not listed explicitly in this table. The best-fit point for the prediction is extracted from a frequentist fit to the data with the Daya Bay 1D constraint on $\sin^2 2\theta_{13}$ [61].

	Neutrino beam			Antineutrino beam	
Sample	ν_μ	ν_e	Low-energy	$\bar{\nu}_\mu$	$\bar{\nu}_e$
$\nu_\mu \to \nu_\mu$	372.3	4.3	0.3	24.4	0.2
$\bar{\nu}_\mu \to \bar{\nu}_\mu$	24.5	0.1	0.0	71.5	0.2
$\nu_\mu \to \nu_e$	0.4	125.3	3.4	0.0	2.1
$\bar{\nu}_\mu \to \bar{\nu}_e$	0.0	1.8	0.1	0.0	18.9
Beam $\nu_e + \bar{\nu}_e$	0.1	26.1	0.8	0.0	6.5
NC	5.5	16.8	5.3	0.8	2.0
Cosmic	4.4	5.5	0.5	0.7	1.1
Others	1.5	0.8	0.1	0.2	0.1
Signal	$397.6^{+26.8}_{-24.2}$	$125.3^{+5.1}_{-5.1}$	$3.4^{+1.0}_{-0.8}$	$96.0^{+5.2}_{-5.7}$	$18.9^{+0.8}_{-0.9}$
Background	$11.0^{+1.3}_{-1.2}$	$55.4^{+2.6}_{-1.7}$	$7.1^{+1.3}_{-1.1}$	$1.7^{+0.2}_{-0.2}$	$12.2^{+0.5}_{-0.7}$
Predicted	408.6	180.7	10.5	97.7	31.1
Observed	384	169	12	106	32

consistent results. The Bayesian fits use uniform priors in the oscillation parameters as plotted (e.g., flat in $\sin^2\theta_{23}$ and $\delta_{\rm CP}$) and Gaussian priors for the systematic parameters, as detailed in [26]. The results from these fits can be marginalized (in the Bayesian framework) or profiled (in the frequentist framework), either simultaneously over both MO (nonconditional) or separately for each MO (conditional). Unless stated otherwise, the results reported in the main text are conditional on the MO and incorporate the 1D Daya Bay constraint on θ_{13}. A comprehensive set of results, including different marginalizations over MO and variations in constraints from Daya Bay, is provided in Supplemental Material [62].

With the increased statistics and updated analysis, NOvA recorded $181\nu_e$ and $384\nu_\mu$ candidates in neutrino mode, and $32\bar{\nu}_e$ and $106\bar{\nu}_\mu$ candidates in antineutrino mode at the FD. The FD spectra resulting from the fitting procedure are shown in Fig. 1 for the neutrino beam, and Table II presents the observed neutrino counts alongside the Monte-Carlo predictions. These predicted values, separated into signal and background subcomponents, are derived from the frequentist best-fit oscillation and systematic parameters. These fits yield $\Delta m^2_{32} = 2.441^{+0.035}_{-0.031} \times 10^{-3}$ eV^2 in the normal MO and $\Delta m^2_{32} = -2.481^{+0.034}_{-0.034} \times 10^{-3}$ eV^2 in the inverted MO. The inverted MO is disfavored at 1.4σ confidence level. The best-fit point for $\delta_{\rm CP}$ is $0.87^{+0.30}_{-0.90}$ π and $\sin^2\theta_{23} = 0.55^{+0.02}_{-0.06}$. The Feldman-Cousins approach [81,82] is used to determine frequentist confidence intervals for the oscillation parameters.

The Bayesian MCMC fits report $\Delta m^2_{32} = 2.431^{+0.036}_{-0.034} \times 10^{-3}$ eV^2 in the normal MO or $\Delta m^2_{32} = -2.479^{+0.036}_{-0.036} \times 10^{-3}$ eV^2 in the inverted MO. The highest posterior density (HPD) for $\delta_{\rm CP}$ is $0.93^{+0.21}_{-0.89}$ π in the normal MO. For both MO, the data favor regions of parameter space close to maximal mixing, $\sin^2\theta_{23} = 0.55^{+0.02}_{-0.06}$, with no significant preference for octant. Figure 2 shows the 90% credible regions in the Δm^2_{32}-$\sin^2\theta_{23}$ plane extracted from this analysis compared to other experiments and previous NOvA results. Good agreement is seen across all the experiments. The goodness of fit is estimated using posterior-predictive p values (PPP), where sampled models

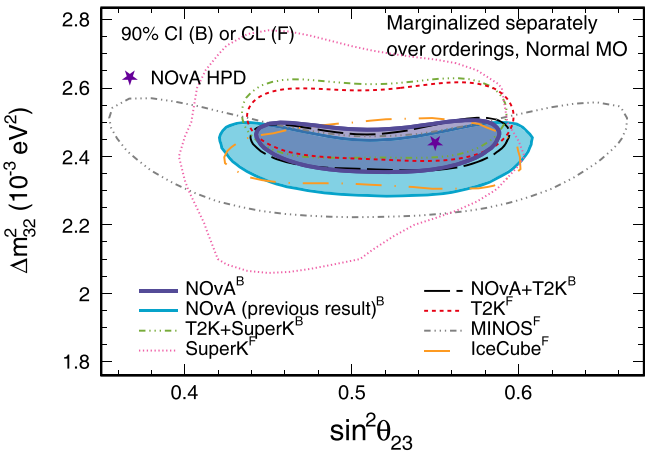


FIG. 2. Comparisons of the 90% intervals for $\Delta m^2_{32} - \sin^2\theta_{23}$ in the normal MO with NOvA 2020 results and superimposed contours from other experiments [84–88], including the 2024 joint NOvA-T2K analysis [89]. The NOvA results are with the 1D Daya Bay constraint on θ_{13} applied [61]. Contours labeled B are from Bayesian analyses, while those labeled F are from frequentist analyses, used when Bayesian results were not available.

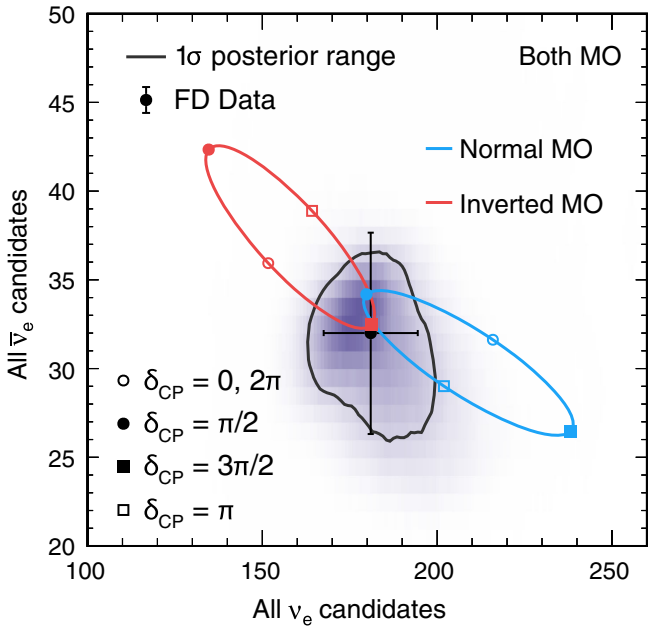


FIG. 3. Bievent plot showing the posterior probability for the predicted number of ν_e and $\bar{\nu}_e$ events in purple, with the 1σ credible interval and the FD data point marked. The two ovals, red for the inverted MO and blue for the normal MO, show the prediction with all the parameters fixed at the NOvA best-fit, varying only δ_{CP}, with four δ_{CP} points marked.

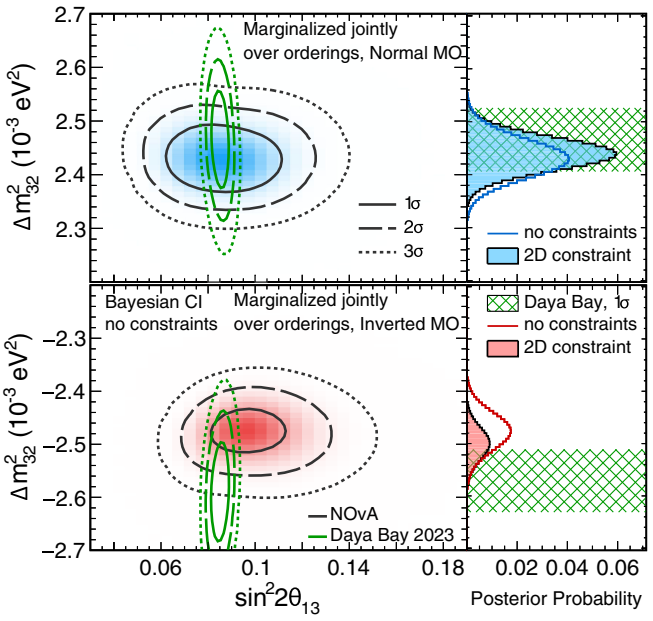


FIG. 4. A comparison of the NOvA and Daya Bay constraints in the $\sin^2 2\theta_{13} - \Delta m^2_{32}$ plane under the assumption of normal (top) or inverted (bottom) MO. The 2D binned NOvA posterior shown in color in the left panels is without any external constraints on θ_{13}. Panels on the right illustrate the effect of applying a 2D $\sin^2\theta_{13} - \Delta m^2_{32}$ constraint from Daya Bay [61] on the MO preference.

that describe the data well will have values close to 0.5 [83]. With the 1D Daya Bay constraint on θ_{13}, the total PPP across all data samples is 0.48, indicating good agreement between the data and the model. The PPP does not change significantly when either no external constraint on θ_{13} is used or when the two-dimensional $\sin^2 2\theta_{13}$–Δm^2_{32} constraint from Daya Bay is applied [62].

The NOvA data lie in the degenerate region of parameter space which can be accommodated within either MO by varying the preferred values of δ_{CP}, as shown in Fig. 3. Bayes factors, representing ratios of posterior probabilities between two hypotheses, are used here to represent how much more probable one model is over another. Bayes factors for the preference of CP violation over CP conservation were extracted using the Savage-Dickey method [90,91] based on the Jarlskog invariant [92], with Jarlskog invariant of 0 representing CP conservation. The Bayes factors for CP violation are 1.1 (containing 51% of the posterior probability) in the normal MO and 4.3 (81%) in the inverted MO, and remain compatible with both CP conservation and CP violation.

This analysis reports the most precise single-experiment measurements of Δm^2_{32}, achieving a fractional uncertainty of 1.5%. This improved precision provides an additional lever for probing the neutrino MO [93,94]. Reactor and long-baseline accelerator measurements of Δm^2_{32} should agree only under the correct MO hypothesis. Figure 4 shows a comparison of the NOvA and the 2D Daya Bay constraints in the $\sin^2 2\theta_{13} - \Delta m^2_{32}$ plane under the two MO hypotheses, with somewhat better agreement in the normal MO. Without any external θ_{13} constraint, NOvA data show a slight preference for normal MO vs inverted MO, with a Bayes factor of 2.4 (70% of posterior probability in favor of normal MO over inverted MO hypothesis). Applying the 1D $\sin^2\theta_{13}$ constraint from Daya Bay [61], this preference increases to 3.3 (77%). When a 2D $\sin^2\theta_{13} - \Delta m^2_{32}$ constraint from Daya Bay is applied, the preference strengthens further to 6.6 (87%). The posterior probability distributions for each are shown in the Supplemental Material [62], and the data release is available at [95].

To conclude, NOvA has reported improved constraints on δ_{CP}, θ_{13}, θ_{23}, and Δm^2_{32} with 10 years of data collected with neutrino and antineutrino beams using enhanced analysis techniques. Notably, NOvA now provides the most precise measurement of Δm^2_{32} to date, with a precision of 1.5%. This enhanced precision in measuring Δm^2_{32} enables the complementarity between accelerator and reactor experiments to be leveraged by incorporating a 2D $\sin^2\theta_{13} - \Delta m^2_{32}$ constraint from Daya Bay, strengthening the preference for the normal MO to 87%. Additional data from current and upcoming neutrino oscillation experiments will help resolve degeneracies, enabling a definitive determination of the MO and the potential discovery of CP violation in the lepton sector. High-precision measurements

of mixing parameters across multiple oscillation channels will also provide a robust test of the three-flavor paradigm in neutrino physics.

Acknowledgments—This document was prepared by the NOvA collaboration using the resources of the Fermi National Accelerator Laboratory (Fermilab), a U.S. Department of Energy, Office of Science, HEP User Facility. Fermilab is managed by Fermi Forward Discovery Group, LLC, acting under Contract No. 89243024CSC000002. This research used resources of the National Energy Research Scientific Computing Center, a DOE Office of Science User Facility supported by the Office of Science of the U.S. Department of Energy under Contract No. DE-AC02-05CH11231 using NERSC Award No. HEP-ERCAP0028967. This work was supported by the U.S. Department of Energy; the U.S. National Science Foundation; the Department of Science and Technology, India; the European Research Council; the MSMT CR, GA UK, Czech Republic; the RAS, the Ministry of Science and Higher Education, and RFBR, Russia; CNPq and FAPEG, Brazil; UKRI, STFC and the Royal Society, United Kingdom; and the State and University of Minnesota. We are grateful for the contributions of the staffs of the University of Minnesota at the Ash River Laboratory, and of Fermilab.

Data availability—The data that support the findings of this article are openly available [95].

[1] B. Pontecorvo, Sov. Phys. JETP **26**, 984 (1968).
[2] S. Bilenky and B. Pontecorvo, Phys. Rep. **41**, 225 (1978).
[3] Z. Maki, M. Nakagawa, and S. Sakata, Prog. Theor. Phys. **28**, 870 (1962).
[4] Y. Fukuda *et al.* (Super-Kamiokande Collaboration), Phys. Rev. Lett. **81**, 1562 (1998).
[5] S. Fukuda *et al.* (Super-Kamiokande Collaboration), Phys. Lett. B **539**, 179 (2002).
[6] Q. R. Ahmad *et al.* (SNO Collaboration), Phys. Rev. Lett. **89**, 011301 (2002).
[7] K. Eguchi *et al.* (KamLAND Collaboration), Phys. Rev. Lett. **90**, 021802 (2003).
[8] D. G. Michael *et al.* (MINOS Collaboration), Phys. Rev. Lett. **97**, 191801 (2006).
[9] M. H. Ahn *et al.* (K2K Collaboration), Phys. Rev. D **74**, 072003 (2006).
[10] K. Abe *et al.* (T2K Collaboration), Phys. Rev. Lett. **107**, 041801 (2011).
[11] Y. Abe *et al.* (Double Chooz Collaboration), Phys. Rev. Lett. **108**, 131801 (2012).
[12] F. P. An *et al.* (Daya Bay Collaboration), Phys. Rev. Lett. **108**, 171803 (2012).
[13] J. K. Ahn *et al.* (RENO Collaboration), Phys. Rev. Lett. **108**, 191802 (2012).
[14] N. Agafonova *et al.* (OPERA Collaboration), Phys. Rev. Lett. **120**, 211801 (2018); **121**, 139901(E) (2018).
[15] S. F. King, A. Merle, S. Morisi, Y. Shimizu, and M. Tanimoto, New J. Phys. **16**, 045018 (2014).
[16] K. Scholberg, J. Phys. G **45**, 014002 (2018).
[17] M. J. Dolinski, A. W. P. Poon, and W. Rodejohann, Annu. Rev. Nucl. Part. Sci. **69**, 219 (2019).
[18] S. Pascoli, S. T. Petcov, and A. Riotto, Phys. Rev. D **75**, 083511 (2007).
[19] G. C. Branco, R. Gonzalez Felipe, and F. R. Joaquim, Phys. Lett. B **645**, 432 (2007).
[20] D. S. Ayres *et al.* (NOvA Collaboration), The NOvA Technical Design Report, Report No. FERMILAB-DESIGN-2007-01, Fermilab, 2007.
[21] P. Adamson *et al.*, Nucl. Instrum. Methods Phys. Res., Sect. A **806**, 279 (2016).
[22] R. L. Talaga, J. J. Grudzinski, S. Phan-Budd, A. Pla-Dalmau, J. E. Fagan, C. Grozis, and K. M. Kephart, Nucl. Instrum. Methods Phys. Res., Sect. A **861**, 77 (2017).
[23] S. Mufson *et al.*, Nucl. Instrum. Methods Phys. Res., Sect. A **799**, 1 (2015).
[24] A. Norman (NOvA Collaboration), J. Phys. Conf. Ser. **396**, 012035 (2012).
[25] M. A. Acero *et al.* (NOvA Collaboration), Phys. Rev. D **106**, 032004 (2022).
[26] M. A. Acero *et al.* (NOvA Collaboration), Phys. Rev. D **110**, 012005 (2024).
[27] S. Agostinelli *et al.* (GEANT4 Collaboration), Nucl. Instrum. Methods Phys. Res., Sect. A **506**, 250 (2003).
[28] GEANT4 Collaboration, https://geant4-data.web.cern.ch/ReleaseNotes/ReleaseNotes4.10.4.html (2017).
[29] L. Aliaga *et al.* (MINERvA Collaboration), Phys. Rev. D **94**, 092005 (2016); **95**, 039903(A) (2017).
[30] J. M. Paley *et al.* (MIPP Collaboration), Phys. Rev. D **90**, 032001 (2014).
[31] C. Alt *et al.* (NA49 Collaboration), Eur. Phys. J. C **49**, 897 (2007).
[32] N. Abgrall *et al.* (NA61/SHINE Collaboration), Phys. Rev. C **84**, 034604 (2011).
[33] D. S. Barton *et al.*, Phys. Rev. D **27**, 2580 (1983).
[34] S. M. Seun, Measurement of $\pi - K$ ratios from the NuMI target, Ph.D. thesis, Harvard University, 2007.
[35] G. M. Tinti, Sterile neutrino oscillations in MINOS and hadron production in pC collisions, Ph.D. thesis, Oxford University, 2010.
[36] A. V. Lebedev, Ratio of pion kaon production in proton carbon interactions, Ph.D. thesis, Harvard University, 2007.
[37] B. Baatar *et al.* (NA49 Collaboration), Eur. Phys. J. C **73**, 2364 (2013).
[38] P. Skubic *et al.*, Phys. Rev. D **18**, 3115 (1978).
[39] S. P. Denisov, S. V. Donskov, Yu. P. Gorin, R. N. Krasnokutsky, A. I. Petrukhin, Yu. D. Prokoshkin, and D. A. Stoyanova, Nucl. Phys. **B61**, 62 (1973).
[40] A. S. Carroll *et al.*, Phys. Lett. **80B**, 319 (1979).
[41] K. Abe *et al.* (T2K Collaboration), Phys. Rev. D **87**, 012001 (2013); **87**, 019902(A) (2013).
[42] T. K. Gaisser, G. B. Yodh, V. D. Barger, and F. Halzen, in *Proceedings of the 14th International Cosmic Ray Conference (ICRC 1975)* (1975), HE Session, Munich, Germany, pp. 2161–2166, Vol. 7.

[43] J. W. Cronin, R. Cool, and A. Abashian, Phys. Rev. **107**, 1121 (1957).
[44] J. V. Allaby *et al.* (IHEP-CERN Collaboration), Phys. Lett. **30B**, 500 (1969).
[45] M. J. Longo and B. J. Moyer, Phys. Rev. **125**, 701 (1962).
[46] B. M. Bobchenko *et al.*, Yad. Fiz. **30**, 1553 (1979) [Sov. J. Nucl. Phys. **30**, 805 (1979)].
[47] V. B. Fedorov, Yu. G. Grishuk, M. V. Kosov, G. A. Leksin, N. A. Pivnyuk, S. V. Shevchenko, V. L. Stolin, A. V. Vlasov, and L. S. Vorobev, Yad. Fiz. **27**, 413 (1978) [Sov. J. Nucl. Phys. **27**, 222 (1978)].
[48] R. J. Abrams, R. L. Cool, G. Giacomelli, T. F. Kycia, B. A. Leontic, K. K. Li, and D. N. Michael, Phys. Rev. D **1**, 1917 (1970).
[49] C. Andreopoulos *et al.*, Nucl. Instrum. Methods Phys. Res., Sect. A **614**, 87 (2010).
[50] C. Andreopoulos, C. Barry, S. Dytman, H. Gallagher, T. Golan, R. Hatcher, G. Perdue, and J. Yarba, arXiv:1510.05494.
[51] J. Nieves, I. R. Simo, and M. J. Vicente Vacas, Phys. Rev. C **83**, 045501 (2011).
[52] R. Gran, J. Nieves, F. Sanchez, and M. J. Vicente Vacas, Phys. Rev. D **88**, 113007 (2013).
[53] B. W. Allardyce *et al.*, Nucl. Phys. **A209**, 1 (1973).
[54] A. Saunders, S. Hoeibraten, J. J. Kraushaar, B. J. Kriss, R. J. Peterson, R. A. Ristinen, J. T. Brack, G. Hofman, E. F. Gibson, and C. L. Morris, Phys. Rev. C **53**, 1745 (1996).
[55] O. Meirav, E. Friedman, R. R. Johnson, R. Olszewski, and P. Weber, Phys. Rev. C **40**, 843 (1989).
[56] S. M. Levenson *et al.*, Phys. Rev. C **28**, 326 (1983).
[57] D. Ashery, I. Navon, G. Azuelos, H. K. Walter, H. J. Pfeiffer, and F. W. Schleputz, Phys. Rev. C **23**, 2173 (1981).
[58] D. Ashery *et al.*, Phys. Rev. C **30**, 946 (1984).
[59] E. S. Pinzon Guerra *et al.* (DUET Collaboration), Phys. Rev. C **95**, 045203 (2017).
[60] A. Aurisano, C. Backhouse, R. Hatcher, N. Mayer, J. Musser, R. Patterson, R. Schroeter, and A. Sousa (NOvA Collaboration), J. Phys. Conf. Ser. **664**, 072002 (2015).
[61] F. P. An *et al.* (Daya Bay Collaboration), Phys. Rev. Lett. **130**, 161802 (2023).
[62] See Supplemental Material at http://link.aps.org/supplemental/10.1103/x53y-2b86 for the energy distributions, posterior-predictive p-values, Bayesian highest-posterior and Frequentist best-fit oscillation parameters, 1D and 2D posterior probability densities, and further comparisons with other experiments. Includes Refs. [63–70].
[63] D. Carabadjac, T2K neutrino oscillation analysis, *Presented at ICHEP 2024* (2024), https://indico.cern.ch/event/1291157/contributions/5888128/attachments/2899009/5083754/T2K_Osc_Analysis_ICHEP_Carabadjac.pdf.
[64] S. Jeon *et al.* (RENO Collaboration), arXiv:2412.18711.
[65] F. P. An *et al.* (Daya Bay Collaboration), Phys. Rev. Lett. **133**, 151801 (2024).
[66] I. Yu, New Results from RENO, Presented at Neutrino-2018 (2018), https://zenodo.org/records/1287949.
[67] M. Gonchar, L. Kolupaeva, and Y. Malyshkin, Neutrino oscillation parameter comparisons, https://git.jinr.ru/nu/osc (2024).
[68] R. E. Kass and A. E. Raftery, J. Am. Stat. Assoc. **90**, 773 (1995).
[69] H. Jeffreys, *Theory of Probability*, 3rd ed. (Oxford University Press, Oxford, England, 1961).
[70] F. James, MINUIT function minimization and error analysis: Reference manual version 94.1, Report No. CERNLIB-D506, CERN, 1994.
[71] L. Alvarez-Ruso *et al.* (NuSTEC Collaboration), Prog. Part. Nucl. Phys. **100**, 1 (2018).
[72] M. Martinez Casales, Constraining neutrino interaction uncertainties for oscillation measurements in the NOvA experiment using Near Detector data, Ph.D. thesis, Iowa State University, 2023, 10.31274/td-20240617-320.
[73] M. Dolce, Constraining neutrino oscillation and interaction parameters with the NOvA Near Detector and Far Detector data using Markov Chain Monte Carlo, Ph.D. thesis, Tufts University, 2023.
[74] J. Calcutt, C. Thorpe, K. Mahn, and L. Fields, J. Instrum. **16**, P08042 (2021).
[75] C. Sweeney, Measurement of the muon neutrino charged-current single charged pion production cross-section in the NOvA Near Detector, Ph. D. thesis, University College London, 2023.
[76] B. J. Jargowsky (NOvA Collaboration), A measurement of ν_e appearance and ν_μ disappearance using 10 years of data from the NOvA experiment, Ph.D. thesis, UC, Irvine, 2024.
[77] B. Roeder, EURISOL Design Study, Report No. 10-25-2008-006 In-beamvalidations.pdf, 2008, pp. 31–44.
[78] Z. Kohley *et al.*, Nucl. Instrum. Methods Phys. Res., Sect. A **682**, 59 (2012).
[79] M. J. Rabelhofer, Study of neutron detector response and related systematic uncertainties in the NOvA oscillation analysis, Ph.D. thesis, Iowa State University, 2023.
[80] R. L. Workman *et al.* (Particle Data Group), Prog. Theor. Exp. Phys. **2022**, 083C01 (2022).
[81] G. J. Feldman and R. D. Cousins, Phys. Rev. D **57**, 3873 (1998).
[82] M. A. Acero *et al.* (NOvA Collaboration), J. Instrum. **20**, T02001 (2025).
[83] A. Gelman, X.-L. Meng, and H. Stern, Statistica Sinica **6**, 733 (1996).
[84] K. Abe *et al.* (T2K and Super-Kamiokande Collaborations), Phys. Rev. Lett. **134**, 011801 (2025).
[85] R. Abbasi *et al.* (IceCube Collaboration), Phys. Rev. Lett. **134**, 091801 (2025).
[86] P. Dunne *et al.* (T2K Collaboration), Oscillation results from Neutrino 2022, Data release, 10.5281/zenodo.6908532 (2022).
[87] P. Adamson *et al.* (MINOS+ Collaboration), Phys. Rev. Lett. **125**, 131802 (2020).
[88] T. Wester *et al.* (Super-Kamiokande Collaboration), Phys. Rev. D **109**, 072014 (2024).
[89] S. Abubakar *et al.* (NOvA and T2K Collaborations), Nature (London) **646**, 818 (2025).
[90] J. M. Dickey, Ann. Math. Stat. **42**, 204 (1971).
[91] J. Mulder, E. J. Wagenmakers, and M. Marsman, arXiv:2004.09899.
[92] The magnitude of CP violation is dependent on all the neutrino mixing angles, rather than δ_{CP} alone, and is dependent on the parametrization of the PMNS matrix. Jarlskog invariant is a rephase-invariant measure,

and therefore more useful in determining non-conservation of the CP symmetry.

[93] H. Nunokawa, S. J. Parke, and R. Zukanovich Funchal, Phys. Rev. D **72**, 013009 (2005).

[94] S. J. Parke and R. Z. Funchal, Phys. Rev. D **111**, 013008 (2025).

[95] S. Abubakar *et al.* (NOvA Collaboration), NOvA 2024 official data release, 10.5281/zenodo.17822359 (2025).